Light Metals 2012 *Edited by: Carlos E. Suarez*
TMS (The Minerals, Metals & Materials Society), 2012

ANODIC BUBBLE BEHAVIOUR IN HALL-HÉROULT CELLS

Kristian Etienne Einarsrud[1], Stein Tore Johansen[2] and Ingo Eick[3]

[1]Department of Energy and Process Engineering, Norwegian University of Science and Technology (NTNU), N-7491 Trondheim, Norway. [2]SINTEF Materials and Chemistry, N-7465 Trondheim, Norway, [3]Hydro Aluminium Deutschland GmbH, 41468 Neuss, Germany

Keywords: Anodic gas bubbles, multiscale modelling, MHD interactions

Abstract

A phenomenological model for the creation and transport of anodic gas bubbles in Hall-Héroult cells is presented. Due to the large variation in length scales and bubble topology, a multiscale approach is introduced in which molecular gas is assumed to be formed as supersaturated CO_2 in the electrolyte. This paper describes models and constitutive relations that are intended for the simulation of anodic bubbles, ranging from the generation of molecular gas species through Faraday's law and subsequent bubble nucleation, to the evolution of macroscopic bubbles by means of a Volume of Fluid (VOF) model. The coupling between macro- and micro scales is performed by means of a population balance. The complete model is implemented in ANSYS FLUENT.

The model is applied to a 2D-cross section of a lab scale electrolysis cell, showing that essential properties are well represented by the proposed approach. Finally, the influence of Lorentz forces on the global bubble behaviour is investigated.

Introduction

As stated in the introduction of the recent review by Cooksey et al. [1], "the contribution of gas bubbles to electrical resistance in aluminium reduction cells is becoming increasingly important as smelters attempt to reduce energy consumption". The importance of anodic gas bubbles arises from their negligible conductivity, effectively screening out sections of an operating anode. For aluminium reduction cell operation, the bubbles can be responsible for as much as 10% of the voltage drop, which is a pure *loss* of energy through Ohmic heating.

The Hall-Héroult cell has a strong dynamic nature due to buoyant bubbles and strong MHD coupling. Hence, it should come as no surprise that the anodic voltage varies with time. A special frequency band ranging from 0.5 to 5 Hz has been credited to bubbles and the produced signal denoted as bubble noise (cf. for instance [2]-[4]).

A detailed experimental description of growth and evolution of single bubbles is given by Xue and Øye [5], identifying three distinct stages. Initially, spherical or semi spherical bubbles are nucleated and grow due to mass transfer. As the inter-bubble distance decreases smaller bubbles begin to merge by coalescence, forming flattened spheroids. Finally, large bubble sheets covering a large fraction of the anode are formed, which, due to buoyancy, release from the anode, marking the end of one bubble cycle.

In practical models the influence of the bubbles is often treated as a gas coverage factor θ and a bubble layer thickness d_b. A microscopic (Lagrangian-type) model for the bubble layer has been developed by Kiss et al. (cf. for instance [3]) over the last decade, allowing for detailed predictions of the gas coverage fraction, which in turn can be used to determine the voltage as a separate calculation.

A principal challenge with Lagrangian models is that one cannot easily handle dynamic interfaces. As a result, Lagrangian bubbles are commonly assumed to be spherical (or circular in 2D), differing from the large bubble sheets believed to form under the anode. In addition, a closure relation for drag-forces must be supplied, if the correct bath-bubble momentum exchange is to be predicted. These relations will necessarily introduce errors if an inadequate bubble topology is used.

An alternative multiphase formalism is the Volume of Fluid (VOF) method, a method developed for the simulation of flows involving interfaces. As the VOF method is a direct approach, momentum exchange terms are obtained as a *result* of the calculated flow field, and closure relations are thus not needed. Furthermore, the VOF method allows for a dynamic evolution and tracking of interfaces with arbitrary shape, as long as the interface is sufficiently resolved.

A transient, fully resolved, VOF modelling approach has recently been introduced (Klaveness et al. [6]), based on molecular gas transport in a porous anode, reproducing the essential voltage behaviour of a laboratory cell. However, due to relatively high computational cost and instabilities for large 3D anodes, an alternative frame-

work based on multiscale modelling and gas transport in the electrolyte has been developed by Einarsrud and Johansen [7]. In the following sections, a brief introduction to the multiscale model is given.

The recent study of Bojarevics and Roy [8] suggest that the presence of electromagnetic forces could significantly influence the overall bubble flow under the anode. In this paper, we follow up these findings by including MHD forces in our proposed model.

Features of proposed model

The proposed gas evolution model is a multiscale approach in which molecular species are produced and transported through a supersaturated electrolyte. Sub grid bubbles are allowed to form through nucleation and the resulting bubble population evolves through mass transfer and coalescence. As sub grid bubbles reach a certain size they are transferred to a macroscopic phase which evolution is governed by a VOF method. Details regarding the model can be found in [7], and only a brief summary of the main features are given in the following.

Gas generation and transport

For simplicity, the production of molecular CO_2 is assumed to be governed by Faraday's law, written in volumetric form as

$$S^p_{CO_2} = \frac{M_{CO_2} \boldsymbol{j} \cdot \boldsymbol{A}}{\nu_e F \mathcal{V}}, \tag{1}$$

where $\boldsymbol{j}$ is the local current density across a unit area $\boldsymbol{A}$ and $\mathcal{V}$ is a unit volume. Although the literature agrees upon the fact that the resulting molecular CO_2 produced on the anode surface (neglecting Boudouard- and back reactions), the path taken by the gas is unclear. As sketched in figure 1, two possibilities exist, namely transport through pores in the anode, or through the bath.

Both processes rely on the fact that either the anode or the bath operates as a gas reservoir. Excluding glassy anodes (cf. for instance Leistra and Sides [9]), both processes are most likely present and the dominating mode will vary, depending upon operational parameters and the relative diffusivities of the bath and anode. From a modelling perspective one mode can be included in the other by adjusting the mass transfer parameters accordingly, yielding the two transport mechanisms equivalent. Thus, until experiments can rule out either of the two modes, the choice of model is of a practical nature based on predictive power, numerical stability, compatibility with other models and computational cost.

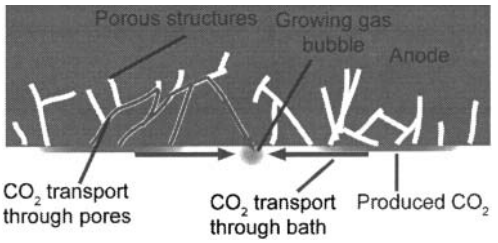

Figure 1: Sketch of the two possibilities for transport of molecular CO_2.

In the proposed model, the bath transport mode is chosen, resulting in the following governing equation for molecular CO_2

$$\frac{\partial C_{CO_2}}{\partial t} + \nabla \cdot (\boldsymbol{u} C_{CO_2} - \mathcal{D}_{eff} \nabla C_{CO_2}) = S^p_{CO_2} - S^n_{CO_2} - S^{dmt}_{CO_2}, \tag{2}$$

where C_{CO_2} is the gas concentration in kg/m^3, $\boldsymbol{u}$ is the bath velocity and $\mathcal{D}_{eff}$ is the effective diffusivity. The source- and sink terms on the right hand side represent production (as of equation 1), nucleation of bubbles and direct mass transfer to existing bubbles, respectively. The production and nucleation sources are active only in computational cells adjacent to the anode surface.

Nucleation of microbubbles

Little is known regarding nucleation in Hall-Héroult cells, regarding both experimental and theoretical investigations. A phenomenological description can however be extracted from the overall information found in the literature. Xue and Øye [5] identify a linear relation between voltage and time during the initial growth of bubbles, corresponding to a linear increase in the projected bubble area with time, i.e. the bubble diameter D_{bub} should obey

$$D_{bub} \propto \sqrt{t}, \tag{3}$$

which is the classical result for a bubble *growing* in a supersaturated solution. In addition, the short time between release and generation of new bubbles (cf. Xue and Øye [5] and Einarsrud and Sandnes [4]) suggests that low to moderate levels of supersaturation are sufficient to initiate bubble nucleation.

This indicates that nucleation relies upon a steady production of gas, rather than abrupt flashing of bubbles expected from classical nucleation. That is, non-classical nucleation as described by Jones et. al [10] appears to describe steady state nucleation in Hall-Héroult cells on a phenomenological level.

According to Xue and Øye, the typical diameter of nucleated bubbles is 0.4-0.6 mm, imposing strict requirements on the mesh if the microbubbles are to be resolved by means of a VOF model. As these requirements make simulations on anything other than a single bubble highly impractical, a multiscale approach is introduced, modelling microscopic sub-grid bubbles up to some size by means of a population balance model (PBM) and large (resolved) bubbles by means of the VOF model.

Evolution of microbubbles

The conservation equation for the number density of the i-th bubble class, $n_i(\boldsymbol{x}, t)$ is given as

$$\frac{\partial n_i}{\partial t} + \nabla \cdot (f(\boldsymbol{u}) n_i - \mathcal{D}_{PBM,i} \nabla n_i) = b_i - d_i, \quad (4)$$

where $f(\boldsymbol{u})$ is an advection function and $\mathcal{D}_{PBM,i}$ is a diffusion tensor. The source and sink terms on the right-hand side respectively represent birth and death rates for the bubble class in question. For the current application, these are determined from nucleation as of Jones et al. [10] (for the smallest bubble class), coalescence as of Luo [11] and mass transfer.

The microbubbles are assumed to be spherical, and are allowed to grow as long as the local bulk concentration exeeds the (prescribed) saturation concentration. The mass flux to a microbubble is given as

$$\dot{\mathcal{M}} = k'(C_{CO_2,B} - C_{CO_2,S}) = k' \Delta C_{CO_2}, \quad (5)$$

where $C_{CO_2,B}$ is the local bulk concentration, obtained by equation 2, and $C_{CO_2,S}$ is the saturation concentration of CO_2. The mass transfer coefficient k' depends upon the local Sherwood number of the flow, thus including both convective and diffusive mass transfer.

In order to span a large range of bubbles using few classes, an exponential discretization based on volume is used, relating the bubble volume of neighbouring classes by

$$V_{i+1} = qV_i. \quad (6)$$

In the current application, $q = 2$.

Coupling to macroscopic bubbles

Given the fields describing the dissolved molecular gas and microscopic bubbles, a coupling model must be introduced in order to handle the transition to macroscopic VOF-bubbles. Considering a population of M bubble classes, the transition can be treated by extending the population with an additional bubble class, which represents the smallest possible concentration of the continuous bubble phase. The additional bubble class is not a true entity of the population it is denoted a ghost class. The volume of a ghost bubble is determined by

$$V_G = qV_m = V_{m+1} \quad (7)$$

which is analogous to the PBM treatment. The number density of ghost bubbles is not determined by a transport equation, but from the volume fraction of the continuous phase, i.e.

$$n_G = \frac{\alpha_g}{V_G}. \quad (8)$$

The rate of change of the ghost class is analogous to that of the microbubbles, that is, ghost bubbles can be formed from growing bubbles or coalescence of two bubbles with volume smaller than V_G. In addition, macroscopic bubbles are allowed to engulf smaller bubbles as they sweep along the anode, in accordance with phenomena observed in water model experiments (cf. Fortin et al. [12]).

The rate of change of the ghost class serves as a mass source for the continuous macroscopic bubbles, defined as

$$S_g = \rho_g V_G \dot{n}_G \quad (9)$$

Thus, once an entity of the population has evolved to the ghost class, it is transferred to the continuous bubble phase from which the VOF model handles the further evolution.

Complete model

In addition to the dissolved gas and dispersed microbubbles treated so far, the continuous flow and electromagnetic fields must be treated. The complete model is shown schematically in figure 2. As seen from the figure, all fields considered are coupled.

The evolution of the k-th phase with density ρ_k is governed by a phase fraction equation on the form

$$\frac{\partial}{\partial t}(\alpha_k \rho_k) + \nabla \cdot (\alpha_k \rho_k \boldsymbol{u}) = S_k \quad (10)$$

where a source on the form of equation 9 is present for the continuous bubble phase. A single flow field is shared between the phases, governed by the incompressible Navier-Stokes equations, that is, gas expansion is neglected. Turbulence is modelled in the continuous phases by means of the realizable k-ϵ model.

Faraday's law (equation 1) requires an electrical current as input. This is obtained from Ohm's law reading

$$\boldsymbol{j} = -\sigma \nabla \phi \quad (11)$$

where σ is the electrical conductivity of the mixture and ϕ is the electrical potential, which is shared between all phases present.

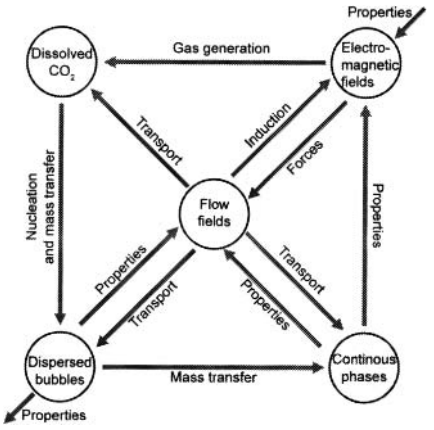

Figure 2: Sketch of elements in complete model and their interaction. Continous- (VOF) and flow-fields are available from ANSYS FLUENT, while remaining nodes and interactions are treated by means of user defined functions and scalars.

Induction currents are neglected as these typically are small in the bath. The electrical potential is determined by the Laplace equation resulting from the conservation of electrical charge. The electrical conductivity of the *electrolyte* is modelled by the Bruggeman equation (cf. [1])

$$\bar{\sigma}_e = \sigma_g \alpha_{PBM} + \sigma_e \left(1 - \alpha_{PBM}\right)^{3/2}, \qquad (12)$$

where $\alpha_{PBM} = \sum_{i=1}^{M} n_i V_i$ is the dispersed bubble phase fraction and σ_i is the conductivity of the i-th pure substance. The *mixture* conductivity is computed as an arithmetic average;

$$\sigma = \sigma_g \alpha_g + \bar{\sigma}_e \left(1 - \alpha_g\right). \qquad (13)$$

Equation 12 thus describes the conductivity of a bath filled cell with a given fraction of microbubbles, while equation 13 describes the conductivity of a cell which includes bath, microbubbles *and* macroscopic bubbles.

MHD forces

A detailed treatment of the *dynamic* magnetic field arising from the changing electrical currents under the anode is beyond the scope of the present work. Instead, similarly to Bojarevics and Roy [8], a simplified magnetic field is used in order to qualitatively investigate its effect. Considering a uniform current density $\boldsymbol{j} = -j_0\hat{z}$, the magnetic field is

$$\boldsymbol{B} = -\frac{\mu_0 j_0}{2}\left(x\hat{y} - y\hat{x}\right). \qquad (14)$$

The resulting Lorentz force, $\boldsymbol{f}_L = \boldsymbol{j} \times \boldsymbol{B}$, is thus directed towards the center of the system, as sketched in figure 3.

Results

In the following, the proposed model is applied to a lab scale electrolysis cell described by Eick et al. [13].

In the experiments a 10 by 10 cm anode was made from industrial carbon and placed in a cylindrical graphite crucible lined with Si_3N_4 with inner diameter 230mm. The anode was fixed to a steel rod so that the anode-cathode distance could be varied. Two of the sides of the anode where fitted with Si_3N_4-plates in order to force gas bubbles to escape in a preferred direction. The whole laboratory cell could be tilted to enhance gas escape further. A simplified sketch of the experimental setup is shown in figure 3.

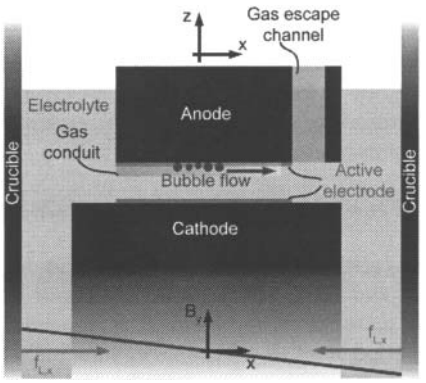

Figure 3: Sketch of experimental cell. A conduit forces bubbles to escape through a designated gas escape channel. The magnitude and sign of the simplified magnetic field and resulting Lorentz force is indicated in bottom of the figure.

All the following simulations are performed using FLUENT version 13.0 (ANSYS Inc., Canonsburg) running on a HP Z800 workstation equipped with two W5590 processors, running at 3.33GHz and 24 GB of RAM. Simulations are transient and restricted to the 2D geometry shown in figure 3. The typical spatial resolution on the anode surface is 1 mm and a time step of 1 ms is used for all simulations. Further details regarding solver settings can be found in [7].

Validation case

As described in Eick et al. [13], several experiments where performed in order to investigate different operational conditions. For the current simulations, the ACD is retained at a constant value of 4 cm, while the anode is tilted at an angle of 2°. The current density is investigated at two levels; $j_0 = 0.8$ A/cm^2 and $j_0 = 1.1$ A/cm^2, resulting, approximately, in a twofold difference in the mean Lorentz-forces.

An analysis of the resulting voltage curves reveals that bubbles typically are responsible for fluctuations of ± 1-3% around the mean voltage, independent of the current density.

As a higher amperage yields a higher gas production rate (as of equation 1), the voltage curves obtained from the high current density cases are expected to have higher dominating frequencies. A FFT of the experimental signals confirms this, typical frequencies being in the range of 0.29-0.37 Hz for $j_0 = 0.8$ A/cm^2, and 0.39-0.61 Hz for $j_0 = 1.1$ A/cm^2.

Figure 4 shows the typical simulated evolution of voltage for each of the two current densities without the presence of Lorentz forces.

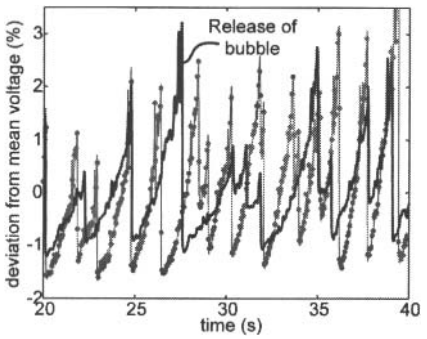

Figure 4: Typical simulated voltage behaviour for $j_0 = 0.8$ A/cm^2 (blue solid line) and $j_0 = 1.1$ A/cm^2 (red dotted line), both with no Lorentz forces present.

Evidently, as seen from figure 4, simulated voltage curves correspond well to those obtained from experiment (cf. Eick et al. [13]). The observed sharp drops in voltage are simultaneous to the release of a bubble into the gas channel, as previously deduced by experiments [4].

The main frequencies for each of the cases considered are 0.27 and 0.68 Hz, respectively, which is very close to the measured frequency ranges.

Influence of MHD forces

Figure 5 corresponds to the simulations shown in figure 4 with Lorentz forces activated.

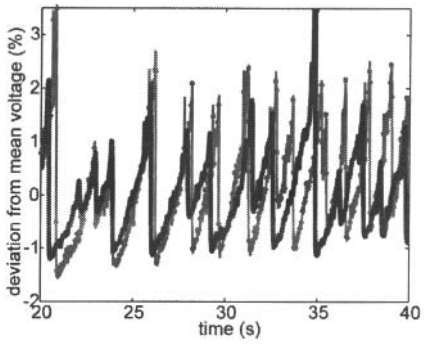

Figure 5: Typical simulated voltage behaviour for $j_0 = 0.8$ A/cm^2 (blue solid line) and $j_0 = 1.1$ A/cm^2 (red dotted line), both with active Lorentz forces.

Comparing figures 4 and 5, the two cases are qualitatively similar. The inclusion of Lorentz forces does not influence the typical magnitude of the oscillations significantly, although localized differences are readily observed. The main frequencies are 0.29 and 0.76Hz, for the two cases considered, that is, the Lorentz forces appear to enhance bubble departure by 7 and 12%, respectively.

As shown by Bojarevics and Roy [8], the pressure contribution from the Lorentz forces is of the form

$$p_L = p_0\,(j_0, L_x) - \alpha\,(j_0, L_x)\,x^2, \qquad (15)$$

where L_x is the length of the anode. Thus, the Lorentz forces yield a slightly favourable pressure gradient on the right half of the anode (cf. figure 3). This results in an increased buoyant force in the region where the concentration of macroscopic bubbles is the greatest, thus promoting increased departure rates and higher frequencies in the voltage signal. Furthermore, due to increased current densities around the shielding gas bubble, strong localized MHD forces potentially contribute to enhanced motion of large bubbles.

Discussion and concluding remarks

This paper describes models and constitutive relations that are intended for the simulation of anodic bubbles in Hall-Héroult cells, in which molecular gas is assumed to supersaturate the electrolyte. Microscopic bubbles are treated by means of a population balance which is coupled to a VOF model for treatment of macroscopic bubbles.

A multiscale approach such as the one presented here involves several parameters which are difficult to measure in a *dynamic* experimental setting. This is for instance the case for the saturation concentration, gas diffusivity and the number of active pores on the anode surface, both strongly dependent upon local features such as bath composition and temperature. Considering for instance the saturation concentration, $C_{CO_2,S}$ (cf. equation 5), changing the value from 0.4kg/m^3 used in the current work to 0.2 kg/m^3, the frequency of the $j_0 = 0.8$ A/cm^2 case increases to 0.49Hz. Due to the strong coupling between various phenomena, it is not possible to determine a single parameter which is more important than the others. Instead, a *set* of relevant parameters which adequately describe the process must be determined by means of a parametric study, an issue which will be an important point for future research.

Comparing to experiments, the behaviour of the anodic gas bubbles is well reproduced, illustrating the potential of the proposed model. For the current study, the inclusion of Lorentz forces does not appear to influence the *global* bubble behaviour significantly, although local effects are readily observed. Bubble departure is found to be slightly enhanced, due to a favourable pressure gradient in regions with high bubble density.

On an industrial scale, Lorentz forces will vary significantly in different regions of the cell, introducing complex 3D-effects not accounted for in the present study. Furthermore, larger scales will involve stronger magnetic fields than the ones considered here, possibly altering the gas transport in a more significant way than that observed in the current setting. Future work will focus on the extension of the proposed model to larger scales, in which these phenomena can be studied.

Finally, it should be emphasized that although the *choice* of the bath transport mode appears to produce sensible results for the current case, detailed experimental investigations are required to determine its the physical significance compared to the anode transport mode.

Acknowledgements

The present work was financed by Hydro Aluminium, Primary Metal Technology with support from the Research Council of Norway. Permission to publish the results is gratefully acknowledged.

References

[1] Cooksey M. A., Taylor M. P. and Chen J. J. J., Resistance Due to Gas Bubbles in Aluminium Reduction Cells. JOM February 2008, 51-57.

[2] Wang X. and Tabereaux A. T., Anodic Phenomena - observations of anode overvoltage and gas bubbling during aluminium electrolysis. Light Metals 2000, 1-9.

[3] Kiss L. I., Poncsak S. and Antille J., Simulation of the bubble layer in aluminium electrolysis cells. Light Metals 2005, 559-564.

[4] Einarsrud K. E. and Sandes E., Anodic voltage oscillations in Hall-Héroult cells. Light Metals 2011, 555-560.

[5] Xue J. and Øye H. A., Bubble behaviour - Cell voltage oscillation during aluminium electrolysis and the effects of sound and ultrasound. Light Metals 1995, 265-271.

[6] Klaveness A., Eick I. and Einarsrud K. E., Gas generation and bubble dynamics underneath carbon anodes. 9th ANSYS Multiphase Flow Conference, Dresden, April 2011.

[7] Einarsrud K. E. and Johansen S. T., On the modelling of anodic bubbles in Hall-Héroult cells. 8th Int. Conf. on CFD in Oil and Gas, Met. and Proc. Ind., Trondheim, Norway, 2011.

[8] Bojarevics V. and Roy A., Bubble transport by electro-magnetophoretic forces at anode bottom of aluminium cells. Light Metals 2011, 549-554.

[9] Leistra J. A. and Sides P. J., Hyperpolarization at Gas Evolving Electrodes - II. Electrochimica Acta, Vol. 33:12, 1988, 1761-1766.

[10] Jones S. F., Evans G. M. and Galvin K. P., Bubble nucleation from gas cavities - a review. Adv. Coll. and Int. Sci., Vol. 80, 1999, 27-50.

[11] Luo H., Coalescence, Breakup and Liquid Circulation in Bubble Column Reactors. PhD Thesis 105, 1993, Norwegian Institute of Technology (NTH).

[12] Fortin S., Gerard M. and Gesing A. J., Physical Modelling of Bubble Behaviour and Gas Release from Aluminium Reduction Cell Anodes. Light Metals 1984, 721-741.

[13] Eick I., Klaveness A., Rosenkilde K., Segatz M. Gudbrandsen H., Solheim A., Skybakmoen E. and Einarsrud K. E., Voltage and Bubble release behaviour in a laboratory cell at low anode-cathode distance, 10th AASTC, 2011, Launceston,Tasmania.